ce/papers Proceedings in civil engineering

Ernst & Sohn A Wiley Brand

ORIGINAL ARTICLE

ibausil F. A. Finger-Institut für Baustoffkunde Bauhaus-Universität Weimar

Low-CO_2 cements based on magnesium oxide / hydromagnesite blends – hydration mechanism and mechanical properties

Frank Winnefeld[1] | Alexander German[1,2] | Pietro Lura[1,2] | Daniel Rentsch[1] | Barbara Lothenbach[1,3]

Correspondence

Dr. Frank Winnefeld
Empa
Laboratory for Concrete & Asphalt
Überlandstrasse 129
8600 Dübendorf
Email: frank.winnefeld@empa.ch

[1] Empa, Dübendorf, Switzerland
[2] ETH Zürich, Zürich, Switzerland
[3] NTNU, Trondheim, Norway

Abstract

Binders based on blends of reactive magnesia and hydromagnesite are low-CO_2 or even carbon-negative cements in case the MgO is generated from magnesium silicates or Mg-containing brines. When MgO is hydrated with water alone, a well crystalline brucite forms, but no measurable strength is developing. In the presence of hydromagnesite, the hydration of MgO is accelerated and the hydrate assemblage is changed. A poorly-crystalline brucite containing some carbonate is the main hydration product. Furthermore, a kind of "gel-water" is observed, which is lost at temperatures above 40-60°C. This brucite-like phase is responsible for strength formation in MgO-hydromagnesite blends. After 28 days, a mortar compressive strength is reached similar to the one of a Portland cement of strength class 32.5.

Keywords

Low-CO_2 binder, magnesium oxide, hydromagnesite, hydration, compressive strength

1 Introduction

A wide range of cementitious binders uses magnesium compounds as key component including Mg-oxychloride, Mg-oxysulfate, Mg-phosphate, Mg-silicate and hydrated magnesium carbonate cements as reviewed by [1, 2]. Up to now, their use is restricted to niche applications. In the recent years, these binders have attracted new interest due the fact that their production can be associated with low CO_2 emissions or might even be carbon-negative. This, however, is only the case, if the MgO used for the binder is not produced from a carbonate-containing raw material such as magnesite [3]. If magnesium silicates such as olivine and serpentine [4, 5] or brines containing magnesium ions [6, 7] are used as precursor of the MgO, the CO_2-balance is much more favourable compared to the conventional calcination process.

One class of Mg-based binders are blends of MgO with hydrated magnesium carbonates (HMCs) such as hydromagnesite ($Mg_5(CO_3)_4(OH)_2{\cdot}4H_2O$ = HY), which have been patented by the "Novacem" start-up venture [8] and could potentially be carbon-negative. Such blends, when mixed with water, set, harden and are able to reach a compressive strength close to the values for construction products based on Portland cement [9-11]. Pure MgO hydrates to form crystalline brucite ($Mg(OH)_2$), but no significant strength is generated. Previous investigations revealed that the brucite formed in the presence of hydromagnesite is of low crystallinity, and it has been suggested that the strength of the hydration products is related to this phase [9, 10]. Further investigations, however, are needed to unravel more details of the hydrate assemblage in such systems.

In the present study, see [12, 13] for more details, the early hydration kinetics is investigated by isothermal calorimetry as well as the strength development of mortar samples. Furthermore, the hydrate assemblage and the pore solution are characterized in detail at temperatures between 7 and 60°C.

2 Materials and Methods

2.1 Materials

Commercial reactive MgO and natural hydromagnesite were used for isothermal calorimetry on pastes and compressive strength measurements on mortars. Various ratios MgO/HY were used. A water/binder ratio of 0.50 was applied, and deionized water was used. A superplasticizer based on polycarboxylate ether (=PCE, solid content 32 mass-%, dosage 3.5 mass-% of binder) was added to achieve sufficient workability. The chemical compositions of the two commercial binder components are shown in Table 1. Quantitative X-ray diffraction analysis (patterns not shown) revealed that the MgO has a phase purity of 94 % (minor phases are lime, portlandite, quartz, hematite, anhydrite). The hydromagnesite contained 65 mass-% hydromagnesite; further phases are 25 mass-% huntite

https://doi.org/10.1002/cepa.2768

($CaMg_3(CO_3)_4$), quartz and dolomite.

For studying the phase assemblage, MgO was produced from $Mg(OH)_2$ in an electrical furnace (6 h at 900°C), and a reagent-grade hydromagnesite was used. Suspensions were prepared using a ratio Mg/HY of 70/30 by mass, ultrapure water and a liquid/solid ratio of 20. Reagent-grade brucite was used as reference.

Table 1 Chemical analyses of commercial MgO and hydromagnesite by X-ray fluorescence analysis.

Parameter	MgO mass-%	Hydromagnesite mass-%
SiO_2	0.38	0.58
Al_2O_3	0.19	<0.11
Fe_2O_3	0.65	0.05
CaO	1.93	6.87
MgO	93.63	38.81
K_2O	0.05	<0.03
Na_2O	<0.06	<0.06
SO_3	0.56	0.08
L.O.I.[a]	2.52	53.48

[a] L.O.I.: loss on ignition

2.2 Methods

For isothermal calorimetry, a TAM Air (TA Instruments) calibrated at 20°C was used. About 6 g of binder were mixed by hand with the appropriate amount of water for a water/binder ratio of 0.50 including the superplasticizer for 2 min using a spatula. The pastes were filled in glass vials, capped and introduced into the calorimeter. Heat flow was recorded for 72 h. The measured data were integrated to determine cumulative heat. Due to the external mixing, the data related to the first 30 min were omitted.

Compressive strength was measured on mortars according to EN 196-1. Curing was done at 20°C and 98% relative humidity.

For the phase analyses, MgO and HY were blended in a ratio of 70/30 by mass, mixed with ultrapure water at a liquid/solid ratio of 20 and sealed-cured at 7, 20, 40 and 60°C up to a sample age of 1 year. At the age of testing, the suspensions were filtered through a 0.45 µm Nylon filter using pressurized air.

The further hydration of the solid residue was stopped by solvent exchange using the protocol described in [14]. Prior to the analyses, the material was ground by hand to a particle size of < 63 µm using an agate mortar.

X-ray diffraction analyses (XRD) were performed in 2θ-range of 5-70° on a PANalytical X'Pert Pro system equipped with CuKα radiation and the X'Celerator detector. Thermogravimetric analyses coupled with infrared spectroscopy of the exhaust gases (TG-IR) were done using a Netzsch STA 449 F3 Jupiter. A heating rate of 10 K/min and nitrogen atmosphere (10 ml/min) were applied. For a semi-quantitative assessment of H_2O and CO_2 content in the exhaust gas, the IR absorbances were integrated in a wavenumber range of 1300-2000 cm^{-1} and 2200-2400 cm^{-1}, respectively. Fourier-transform infrared (FT-IR) spectroscopy was performed using a Bruker ALPHA II FTIR-ATR instrument using the ATR (attenuated total reflection) technique in a wavenumber range of 4000-600 cm^{-1} at a resolution of 4 cm^{-1}. ^1H-^{13}C cross-polarization magic angle spinning nuclear magnetic resonance spectroscopy (^{13}C CP-MAS NMR) was conducted with a Bruker Advance III 400 NMR spectrometer on a 7 mm MAS NMR probe. MAS rotation was set to 4000 Hz, contact time to 2 ms, and repetition time to 3 s.

pH-values of the liquid phase were measured on the undiluted solutions with a Knick pH meter 766, calibrated with buffer solutions between a pH of 9 and 12. Inorganic carbon was measured on diluted samples using a Sievers 5310C TOC analyzer. Na, K, Mg, Ca, SO_4 and Cl concentrations were measured on diluted samples with ion chromatography (IC) using a Dionex ICS-3000 instrument.

Thermodynamic calculations were performed using the geochemical software GEMS [15, 16] coupled with the Nagra/PSI thermodynamic database [17] and additional data related to magnesium carbonates [10, 18].

3 Results

3.1 Hydration kinetics and strength development

Figure 1 shows the hydration heat flow of MgO/hydromagnesite pastes compared to a pure MgO paste. All pastes contained PCE-superplasticizer. Previous work showed that the PCE does not induce a strong retardation in such a binder, which is different to systems based on Portland cement [10]. Hydromagnesite strongly accelerates the hydration of MgO, as it is suggested to act as nucleation seed [19]. The effect increases at a higher replacement of MgO by hydromagnesite.

The development of cumulative heat shows that hydromagnesite has a significant impact on the reaction degree of MgO during the first three days of hydration (Figure 2). From the hydration enthalpy of MgO (930 J/g [20]), reaction degrees of 48%, 66% and 89% after 72 hours can be estimated for pure MgO, MgO/HY 90/10 and MgO/HY 70/30, respectively.

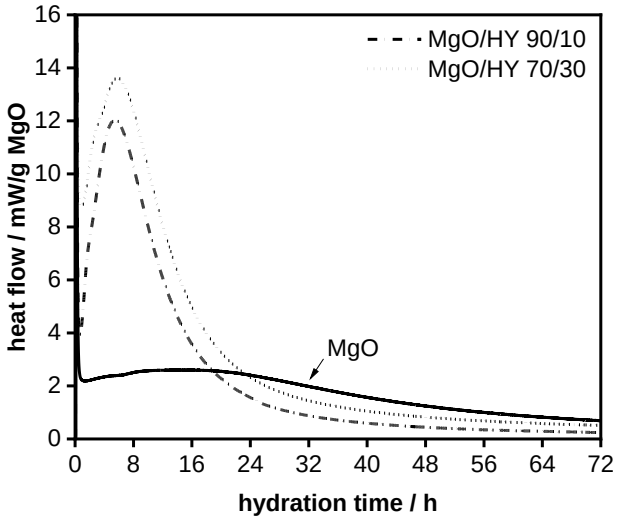

Figure 1 Hydration heat flow of MgO and MgO/HY pastes (commercial raw materials, water/binder 0.50, referred to 1 g of Mg) in mW/g MgO.

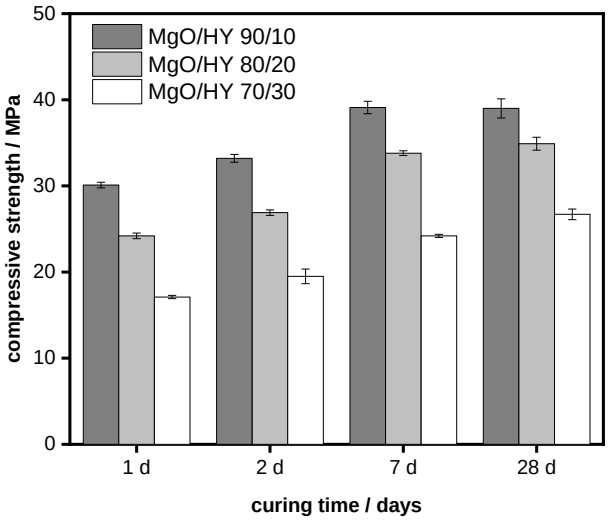

Figure 3 Compressive strengths of MgO/HY mortars (commercial raw materials). The mortar with pure MgO as binder did not develop measurable strength.

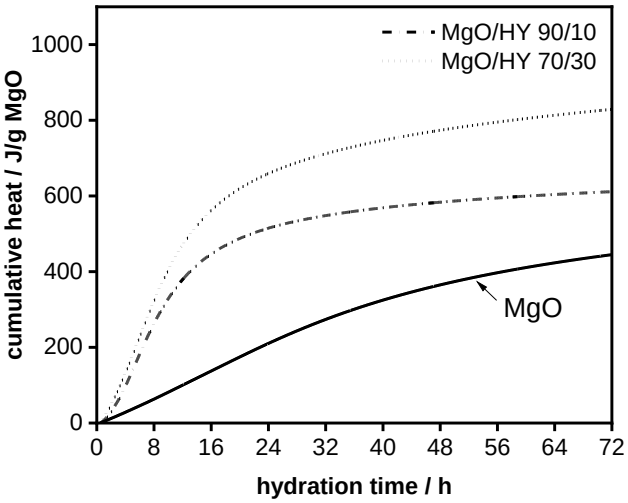

Figure 2 Hydration heat of MgO and MgO/HY pastes (commercial raw materials, water/binder 0.50) in J/g MgO.

The mortar with pure reactive MgO as binder did not develop any strength. When a part of the MgO is replaced by hydromagnesite, the mortars set and harden. The main development of compressive strength takes place during the first day of curing (Figure 3). Afterwards, only a rather slow gain of strength is observed. Compressive strength decreases with increasing replacement of MgO by hydromagnesite. There must be a strength optimum between 0 and 20 mass-% replacement, as pure MgO does not develop strength. The MgO/HY 90/10 mixture reaches after 28 days a compressive strength comparable to a Portland cement of strength class 32.5.

3.2 Hydrate assemblage

The X-ray diffraction patterns of the suspensions cured for one year are displayed in Figure 4. After one year of curing, hydromagnesite is still present at all investigated temperatures. Brucite forms as main hydration product. Its reflections are broader and shifted compared to those of the reagent-grade brucite in agreement with earlier work [9, 10]. This refers especially to the 001 reflection, which is shifted to higher 2ϴ-values with decreasing curing temperatures. For the sample cured at 60°C, the position is the same as for the reagent-grade brucite.

A small hump occurs at 16.1-16.8° 2ϴ CuKα for the samples cured at 7 and 20°C. This hump had previously been tentatively assigned to an unknown phase [9, 10]. The hump shifts to a higher 2ϴ-value for the 40°C sample, where it is visible only as a shoulder of the 001 brucite reflection, and vanishes for the 60°C sample

TGA-IR data of the MgO/HY 70/30 suspension cured at 20°C and at 60°C for one year are shown in Figure 5. The mass losses of the sample cured at 20°C can be mainly assigned to brucite and hydromagnesite. About 50-75% of the HY has reacted, rather independently from the curing temperature, as obtained from mass balance calculations based on TGA-IR and verified by ^{13}C CP-MAS NMR.

Between 300 and 480°C, the decomposition temperature of brucite, not only H_2O, but also CO_2 is released. The CO_2 release cannot be explained just by the decomposition of hydromagnesite. Thus, either an unknown carbonate phase must be present, or the brucite contains some carbonate. Furthermore, a mass loss is observed at 30-160°C for the 20°C sample in agreement with [10], which cannot be assigned to brucite or any known magnesium carbonate. A water loss at such a low temperature indicates the presence of loosely bound water. This mass loss is not evident for the sample cured at 60°C.

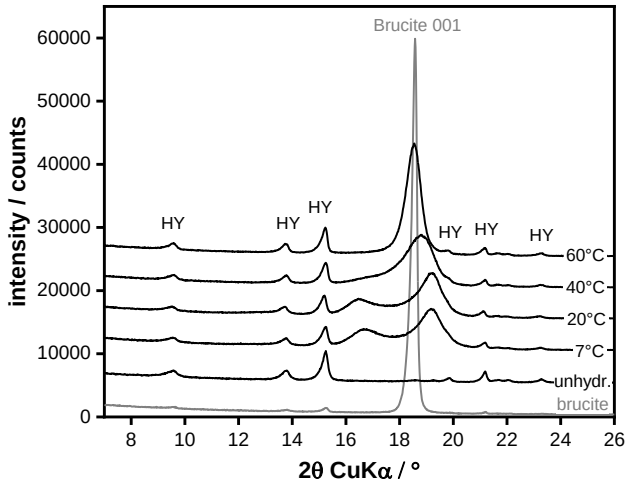

Figure 4 XRD patterns of the solid part of the MgO/HY 70/30 suspensions (reagent-grade materials) cured at 7, 20, 40, and 60°C for one year. Unhydrated binder and reagent-grade brucite as references.

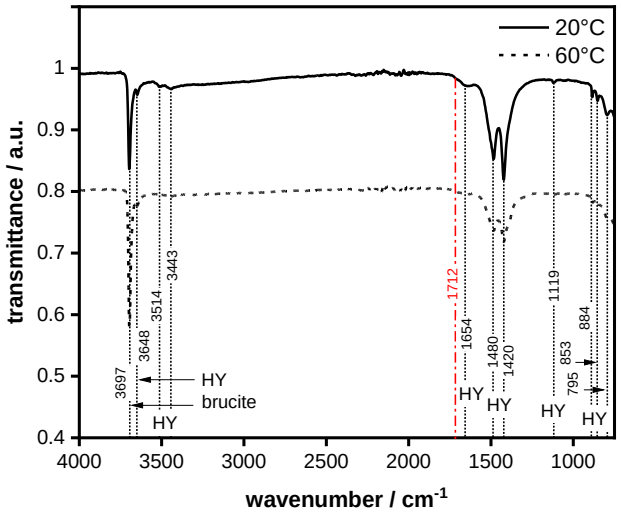

Figure 6 IR spectra of the solid part of the MgO/HY 70/30 suspensions (reagent-grade materials) cured at 20 and 60°C for one year. The red dash-dotted line marks the weak band of unknown origin.

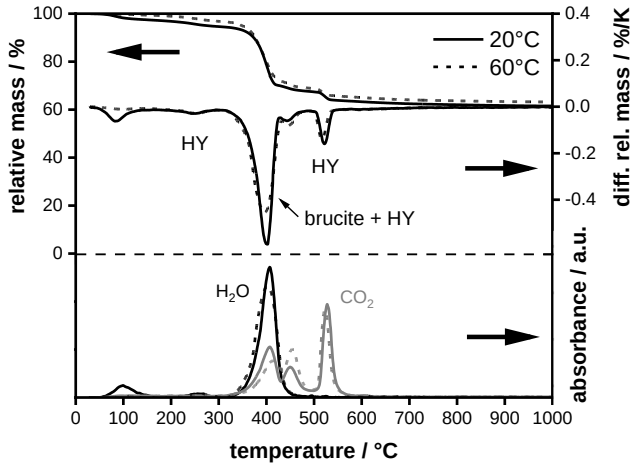

Figure 5 TGA-IR of the solid part of the MgO/HY 70/30 suspensions (reagent-grade materials) cured at 20 and 60°C for one year.

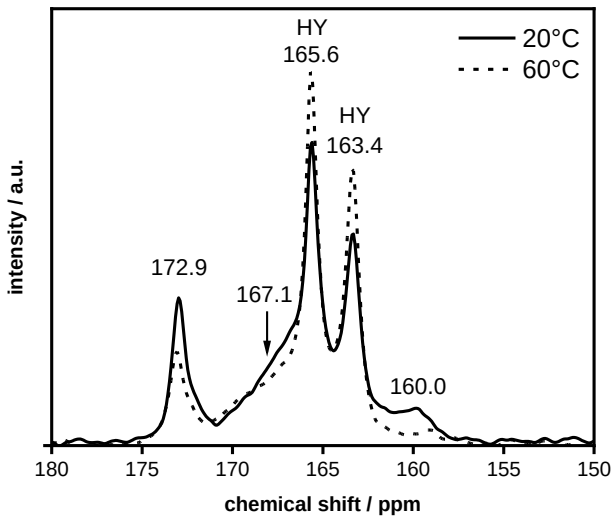

Figure 7 ^{13}C CP-MAS NMR spectra of the solid part of the MgO/HY 70/30 suspensions (reagent-grade materials) cured at 20 and 60°C for one year.

Figure 6 provides the IR-spectra of the MgO/HY 70/30 suspensions cured at 20 and 60°C for one year. The major bands can be assigned either to brucite or to hydromagnesite [21-25]. A weak band of unknown origin is observed at a wavenumber of 1712 cm^{-1}, which is probably the result of an asymmetric stretching vibration of a carbonate. Tentatively, this vibration is assigned to an unknown carbonate phase. The band is also observed in the sample cured at 60°C.

The ^{13}C CP-MAS NMR spectrum (Figure 7) of the sample cured at 20°C shows two signals for hydromagnesite (163.4 ppm and 165.6 ppm) and a signal at 167-168 ppm. A signal at a similar position in a clay-containing system was tentatively assigned to sorbed HCO_3^- [18], however the signal might be of different origin in our system. Two further resonances at 159.4-160.0 ppm and at 173 ppm could not be assigned to any known magnesium carbonate phase. Thus, they might be related to an unknown phase. The signals of the 60°C sample are very similar to those at 20°C.

The analyses of the liquid phase are shown in Table 2. The concentrations of dissolved inorganic carbon and magnesium increase with increasing temperature, while the pH value decreases.

The pore solution data was used to calculate effective saturation indices [26] for brucite and hydrated magnesium carbonates (Table 3). As expected, magnesite is highly oversaturated at all investigated temperatures, but it does not form at the temperatures studied due to kinetic reasons. Artinite ($Mg_2(CO_3)(OH)_2 \cdot 3H_2O$), brucite and hydromagnesite are oversaturated as well. Dypingite ($Mg_5(CO_3)_4(OH)_2 \cdot 5H_2O$) is near saturation. Due to their oversaturation, artinite or dypingite would be stable. However, they are not identified in agreement with [9, 10], indicating a kinetic hindrance in formation or some uncertainties of their thermodynamic data. Lansfordite ($MgCO_3 \cdot 5H_2O$) and nesquehonite ($MgCO_3 \cdot 3H_2O$) are undersaturated and not identified. Based on the solution

chemistry, the ion activity products of various hypothetical hydrated magnesium carbonates, whose compositions were derived from mass balance calculations, were calculated (data not shown). The calculations revealed that these hypothetical phases were unstable compared to a mix of brucite and hydromagnesite of the same bulk composition. Thus, it can be suggested that the carbonate and the water are bound in a brucite-like phase of low crystallinity.

Table 2 Composition of the liquid phase of MgO/HY 70/30 suspensions (reagent-grade materials) cured at 7, 20, 40, and 60°C for one year. Values in mmol/l except for pH. pH was measured at 23±1 °C and recalculated to the respective temperatures.

Parameter	7°C	20°C	40°C	60°C
Na	0.533	0.571	0.599	0.634
K	0.013	0.016	0.015	0.017
Mg	1.479	1.330	1.481	1.911
Ca	0.048	0.049	0.047	0.053
SO_4	0.438	0.443	0.533	0.715
Cl	0.087	0.085	0.096	0.018
DIC[a]	1.507	1.390	1.573	1.947
OH^-	0.15	0.11	0.08	0.07
pH	10.8	10.2	9.5	8.8

[a] DIC: dissolved inorganic carbon

Table 3 Effective saturation indices of relevant hydrate phases of MgO/HY 70/30 suspensions (reagent-grade materials) cured at 7, 20, 40, and 60°C for one year. Positive values = oversaturation, negative values = undersaturation.

Phase	7°C	20°C	40°C	60°C
Brucite	+0.2	+0.5	+0.8	+0.8
Magnesite	+1.8	+1.9	+2.1	+2.1
Lansfordite	-0.9	-1.1	-1.2	-1.7
Nesquehonite	-1.1	-1.1	-1.0	-1.1
Artinite	+0.8	+0.8	+1.0	+0.8
Hydromagnesite	+0.1	+0.2	+0.4	+0.4
Dypingite	-0.4	-0.3	±0.0	±0.0

4 Conclusions

Reactive magnesia hydrates to a well-crystalline brucite. This reaction does not lead to a significant strength formation.

The addition of hydromagnesite accelerates the reaction of MgO, and the main hydration product is brucite with a low crystallinity. The dissolution of a part of the hydromagnesite during hydration provides carbonate ions; however, no known hydrated magnesium carbonate phase could be identified. Based on these results, it is therefore suggested that the brucite formed in such systems contains some carbonate. The small hump in the XRD pattern at ≈ 16.1-18.8° 2θ CuKα is tentatively assigned to this brucite-like phase. Furthermore, thermogravimetric data shows a significant mass loss in the region of approximately 30-160°C, which is associated with the loss of loosely bound water. Tentatively this water is assigned as a kind of "gel-water" within the low-crystalline brucite. This "gel-water" cannot be identified in samples cured at 60°C, while the carbonate associated with brucite is still present, but probably in lower amounts.

The carbonate-containing brucite phase is responsible for strength formation in MgO-hydromagnesite binders. The blend with 90 mass-% MgO and 10 mass-% hydromagnesite reached a compressive strength of 39 MPa after 28 days when tested on mortars according to EN 196-1.

Acknowledgements

The authors acknowledge Ellina Bernard, Yiru Yan and Luigi Brunetti for their support.

References

[1] Walling, S.A.; Provis, J.L. (2016) *Magnesia-based cements: A journey of 150 years, and cements for the future?.* Chemical Review 116, p. 4170-4204.

[2] Bernard E.; Nguyen, H.; Scott, A.; Kawashima, S.; Provis, J.L.; Manzano, H.; Unluer, C.; Lothenbach, B.; Winnefeld, F.; Kinnunen, P. (2023) *MgO-based cements – Current status and opportunities*. RILEM Technical Letters, submitted.

[3] Gartner, E.; Sui, T. (2018) *Alternative cement clinkers*. Cement and Concrete Research 114, p. 27-39.

[4] Scott, A.; Oze, C.; Shah, V.; Yang, N.; Shanks, B.; Cheeseman, C.; Marshall, A.; Watson, M. (2021) *Transformation of abundant magnesium silicate minerals for enhanced CO_2 sequestration*. Communications Earth & Environment 2, p. 25.

[5] Zevenhoven, R.; Slotte, M.; Koivisto, E.; Erlund, R. (2017) *Serpentinite carbonation process routes using ammonium sulfate and integration in industry*. Energy Technology 5, p. 945-954.

[6 Chu, S.H.; Yang, E.H.; Unluer, C. (2023) *Chemical synthesis of magnesium oxide (MgO) from brine towards minimal energy consumption*. Desalination 556, 116594.

[7] Badjatya, P.; Akca, A.H.; Alvarez, D.V.F., Chang, B.; Ma, S.; Pang, X.; Wang, E.; van Hinsberg, Q.; Esposito, D.V.; Kawashima, S. (2022) *Carbon-negative cement manufacturing from seawater-derived magnesium feedstocks*. Proceedings of the National Academy of Sciences of the United States of America 119, e2114680119.

[8] Vlasopoulos, N.; Cheeseman, C.R. (2009) *Binder composition*. PCT Patent Application PCT/GB2009/001610, International Publication Number WO 2009/156740 A1 (12/30/2009).

[9] Kuenzel, C.; Zhang, F.; Ferrándiz-Mas, V.; Cheeseman, C.R.; Gartner, E.M. (2018) *The mechanism of hydration of MgO-hydromagnesite blends*. Cement and Concrete Research 103, p. 123-129.

[10] Winnefeld, F.; Epifania, E.; Montagnaro, F.; Gartner, E.M. (2019) *Further studies of the hydration of MgO-hydromagnesite blends*. Cement and Concrete Research 126, 105912.

[11] Winnefeld, F.; Leemann, A.; German, A.; Lothenbach, B. (2022) *CO_2 storage in cement and concrete by mineral carbonation*. Current Opinion in Green and Sustainable Chemistry 38, 100672.

[12] German, A.; Winnefeld, F.; Lura, P.; Rentsch, D.; Lothenbach, B. (2023) *Hydrous carbonate-containing brucite (HCB) in MgO / hydromagnesite blends*. Cement and Concrete Research, submitted.

[13] German, A. (2023) *Potential use of a low-carbon magnesia (MgO) binder for construction purposes*, PhD Thesis, ETH Zürich, Switzerland.

[14] Snellings, R.; Chwast, J.; Cizer, O.; De Belie, N.; Dhandapani, Y.; Durdzinski, P.; Elsen, J.; Haufe, J.; Hooton, D.; Patapy, C.; Santhanam, M.; Scrivener, K.; Snoeck, D.; Steger, L.; Sui, T.; Vollpracht, A.; Winnefeld, F.; Lothenbach, B. (2018) *RILEM TC-238 SCM recommendation on hydration stoppage by solvent exchange for the study of hydrate assemblages*. Materials and Structures 51, p. 172.

[15] Wagner, T.; Kulik, D.A.; Hingerl, F.F.; Dmytrieva, S.V. (2012) *GEM-Selektor geochemical modelling package: TSolMod Library and data interface for multicomponent phase models*. Canadian Mineralogist 50, p. 1173-1195.

[16] Kulik, D.A.; Wagner, T.; Dmytrieva, S.V.; Kosakowski, G.; Hingerl, F.F.; Chudnenko, K.V.; Berner, U.R. (2013) *GEM-Selektor geochemical modeling package: revised algorithm and GEMS3K numerical kernel for coupled simulation codes*. Computational Geosciences 17, p. 1-24.

[17] Hummel, W.; Berner, U.; Curti, E.; Pearson, F.J.; Thoenen, T. (2002) *Nagra/PSI chemical thermodynamic data base 01/01*. Radiochimia Acta 90, p. 805-813.

[18] Bernard, E.; Lothenbach, B.; Rentsch, D.; German, A.; Winnefeld, F. (2022) *Effect of carbonates on the formation of magnesium silicate hydrates*. Materials and Structures 55, p. 183.

[19] Dung, N.T.; Unluer, C. (2017) I*nfluence of nucleation seeding on the performance of carbonated MgO formulations*. Cement and Concrete Composites 83, p. 1-9.

[20] Thomas, J.J.; Musso, S.; Prestini, I. (2014) *Kinetics and activation energy of magnesium oxide hydration*. Journal of the American Ceramic Society 97, p. 275-282.

[21] Jones, G.C.; Jackson, B. (1993) *Infrared Transmission Spectra of Carbonate Minerals*. London (UK), New York (US): Chapman & Hall.

[22] Frost, R.L.; Kloprogge, J.T. (1999) *Infrared emission spectroscopic study of brucite*. Spectrochimica Acta Part A -Molecular and Biomolecular Spectroscopy 55, p. 2195-2205.

[23] Frost, R.L. (2011) *Raman spectroscopic study of the magnesium carbonate mineral hydromagnesite ($Mg_5(CO_3)_4$ $(OH)_2{\cdot}4H_2O$)*. Journal of Raman Spectroscopy 42, p. 1690-1694.

[24] Han, H.; Hu, S.; Feng, J.; Gao, H. (2011) *Effect of stearic acid, zinc stearate coating on the properties of synthetic hydromagnesite*. Applied Surface Science 257, p. 2677-2682.

[25] Chukanov, N.V.; Chervonnyi, A.D. (2016) *Infrared Spectroscopy of Minerals and Related Compounds*. Cham (CH), Heidelberg (GER), New York (US), Dordrecht (NL), London (UK): Springer.

[26] Lothenbach, B. (2010) *Thermodynamic equilibrium calculations in cementitious systems*. Materials and Structures 43, p. 1413-1433.